HiSST: 2nd International Conference on
High-Speed Vehicle Science Technology
11–15 September 2022, Bruges, Belgium

Experimental Assessment of a Flush Air Data Sensing System for the Hypersonic Flight Experiment HEXAFLY-INT

J. Riehmer[1], A. Gülhan[2], J. Steelant[3]

Abstract

In the frame of the HEXAFLY-INT project [5, 6] a Flush Air Data Sensing system (FADS) was design to determine the flight angles, Mach number and altitude of a hypersonic waverider. Within this study an extensive experimental study was performed of a 2:1 nose model in the supersonic (TMK) and hypersonic (H2K) wind tunnel at the DLR in Cologne to evaluate this concept. Main focus was set on pressure measurements for various angles of attacks and sideslip as well as different Mach numbers and Reynolds numbers along the expected trajectory of the flight vehicle. Additional understanding about the flow around the nose of the vehicle was obtained by using schlieren imaging and oil film visualization. A comparison between analytic and numeric predictions from the design study and the measured data during this study show a good agreement and proofed the feasibility of the FADS design for wind tunnels and give confidence for the use under real flight conditions. This study concludes with an assessment on how to improve the FADS algorithms by using wind tunnel data.

Keywords: *Flush Air Data Sensing System, Wind Tunnel Testing, HEXAFLY*

1. Introduction

An Air Data Systems is a commonly known system of multiple pressure sensors which are processed in order to get the angle of attack, angle of sideslip, Mach number and pressure (altitude). It is used in wind tunnels in form of a 5-hole probe or in commercial/military aircrafts. For super and hypersonic vehicles protrusions into the flow have a significantly bad influence on the aerodynamics and aerothermodynamics. In order to avoid this downside the sensors are integrated into the surface of the vehicle and the ADS becomes a flush ADS (FADS). Since the shape of supersonic vehicles is very individually each FADS require an individual adaptation of the system onto the specific vehicle in terms of designs as well as calibration and validation.

Flush Air Data Sensing systems where used in different applications like supersonic military aircrafts (NASA) [7], reentry capsules [4] and Hypersonic aircrafts [1,8]. DLR tested and evaluated this technology recently for SHEFEX II [3] and ROTEX-T [2].

1.1. HEXAFLY-INT FADS

Fig 1 shows a sketch of the HEXAFLY-INT vehicle with e position of the FADS is marked in green. Basically, the front position was chosen to have the most undisturbed flow with no vortexes or "shadowing" regions. Further pressure sensors on the vertical tails and the body of the vehicle will be installed to cross-check and validate the inputs acquired with the FADS. The pressure sensors positions were evaluated using a theoretical and semi-empirical/numerical approach and the design principle is

[1] *Research Scientist, DLR Institute of Aerodynamics and Flow Technology, Supersonic and Hypersonic Technologies Department, Cologne, Germany, johannes.riehmer@dlr.de*

[2] *Head of Department, DLR Institute of Aerodynamics and Flow Technology, Supersonic and Hypersonic Technologies Department, Cologne, Germany, ali.guelhan@dlr.de*

[3] *ESA-ESTEC, Flight Vehicles and Aerothermodynamics Engineering Section TEC-MPA, P.O. Box 299, Noordwijk, Netherlands, Johan.Steelant@esa.int*

introduced in detail in another study. In Fig 1 on the right side the positions are shown for the downscaled wind tunnel model. Here the black line indicates the leading edge along the nose of the vehicle. Sensors 6 and 10 are used for angle of attack detection, since these positions quite close to the leading edge are sensitive to angle of attack variations and less sensitive to sideslip variations. Sensors 3 and 8 are used as backup sensors for the 6 and 10 sensors. The other sensors are placed in positions sensitive to sideslip variations. Always a certain distance is kept from the leading edge to avoid its negative effects on the pressure measurements.

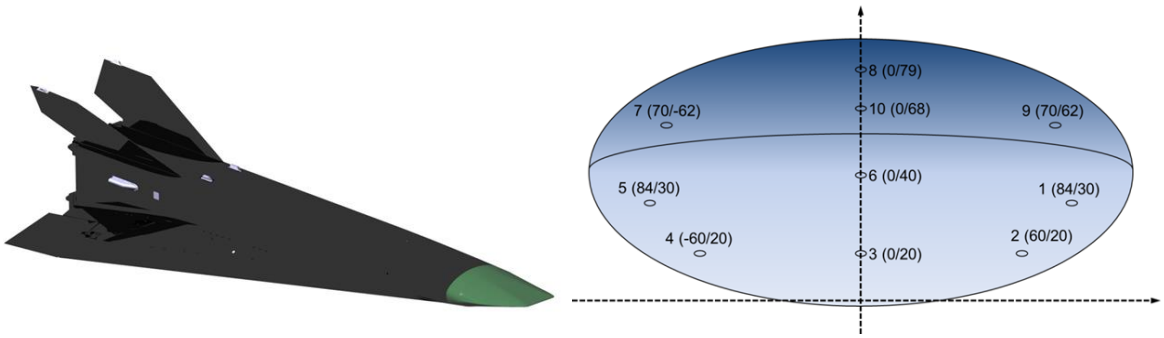

Fig 1: FADS position (green) in the HEXAFLY-INT vehicle and sensor position in the nose

2. Wind Tunnel Model and Test Procedures

2.1. Facilities

As mentioned, the H2K and TMK wind tunnel at the DLR in Cologne was used to reproduce the flight envelop plotted in Fig 4. Both wind tunnels are blow down wind tunnel supplied by a high-pressure air supply. This air is led thru a Laval nozzle into the measurement chamber and released thru a diffusor. For the TMK the air is released into a free atmosphere while for the H2K the air flow from the diffusor is sucked into a vacuum sphere, allowing the facility to operate at ambient pressures down to a few mbar. A further difference is the size of Laval nozzle which is 600mm in diameter in the case of H2K and 600x600mm rectangular in the case of the TMK. Optional the TMK can be operated in transonic and subsonic conditions, but which were not used during this campaign. In Fig 2 a sketch of both facilities is shown.

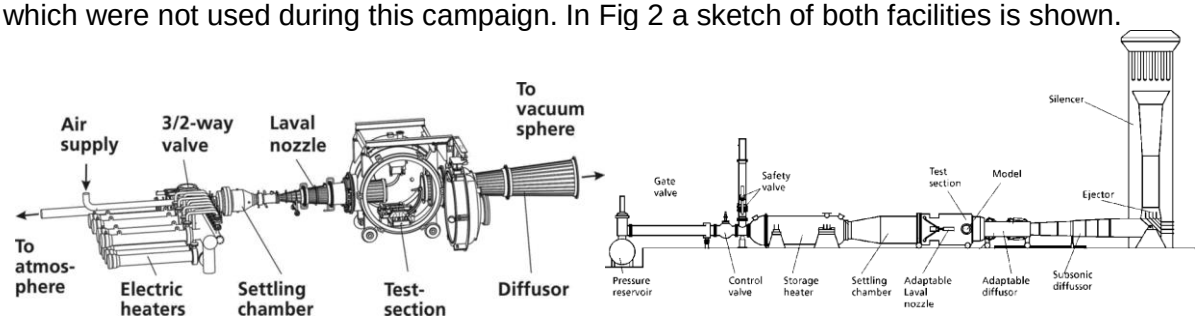

Fig 2: Sketch of H2K (left) and TMK (right) facility

2.2. Wind Tunnel Model and Instrumentation

Wind tunnel model was designed for experiments in the supersonic wind tunnel TMK as well as in the hypersonic wind tunnel H2K. Due to the size of the original HEXAFLY-INT vehicle the model was downsized by a factor of 2. The scaling of the model was chosen to get as close as possible to the flight size of the vehicle in order to get Reynolds numbers close to the expected values to the critical phases of the flight.

Fig 3 on the left side shows a technical drawing of the model mounted on a sting. On the right side a sketch of the implementation of the sensors in the model is shown. The mounting was changed slightly in comparison to the flight vehicle due to the scaling and accessibility. The pressure is measured with a flush pressure port on the surface with a hole of a diameter of 0.5mm. A metallic insert glued into the model was used to mount a metallic adapter which was

connected to the pressure measurement module via a flexible hose. For each pressure port an absolute pressure sensor was used and no differential sensors were implemented.

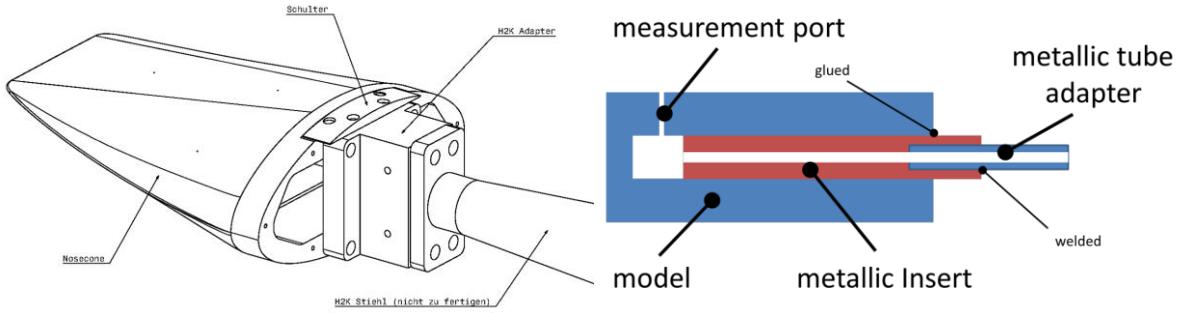

Fig 3: Wind tunnel model of the HEXAFLY-INT and implementation of measurement ports

The pressure tubes were connected to a *PSI pressure scanner* with a range of 45 psi (~3 Bar) for the TMK experiments while in the H2K a *DTC Initium 15 PSID DTC 32 Port scanner* for the lower pressures in the H2K was used. In order to visualize the flow both wind tunnels provide a schlieren image installation.

2.3. Test Matrix

The main goal of experimental investigations was to collect an extensive experimental data base of the relevant angle of attack and sideslips for the relevant Mach numbers and Reynolds numbers. In Fig 4 the investigated flight path of the HEXAFLY-INT vehicle during reentry from Mach 7 down to Mach 1.5 is shown. The target points (stars) with respect to Mach number are shown together with the operation regime of the wind tunnels (with respect to Mach number). On the right side of Fig 4 the red arrows indicate the (continuously) span of angle of attack, angle of sideslip and combined variation during an individual run of the wind tunnel. During one wind tunnel run the angle of attack and sideslip were varied in both directions (back and forth) along the red lines. Hereby the combined variation was achieved by rolling the model by 45°. The full span of angle of attack variation was only performed in the H2K since here the data was necessary due to the intended pullout maneuver of the real flight vehicle. For the TMK angle of attack was only varied between -5° and +5° in order to avoid blocking of the wind tunnel.

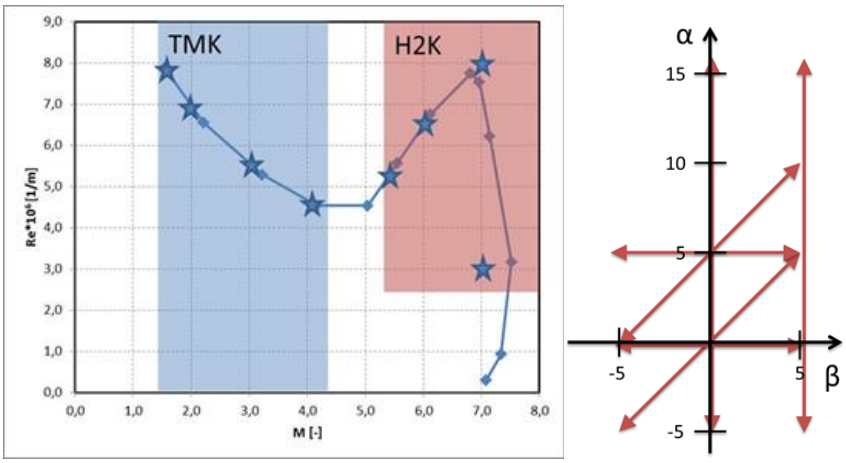

Fig 4: Basic schematic of the investigated flight regime and investigated angle of Attack and sideslip variation

2.4. Test Procedure

The test configurations in both wind tunnels were quite similar. The model was mounted onto a sting inside the wind tunnel and was swept by variation of angle of incidence around the rotation point which was within the model. Fig 5 on the left side shows the typical curve of the measurement. The black lines indicate pressure measurement on the wind side (solid) and leeside (dashed) of the model together with the variation of the incidence angle (red). In order

to get the angle of attack the roll angle around the sting was 0°, for getting angle of sideslip the roll angle was set to 90° and for combined variation it was set to 45°.

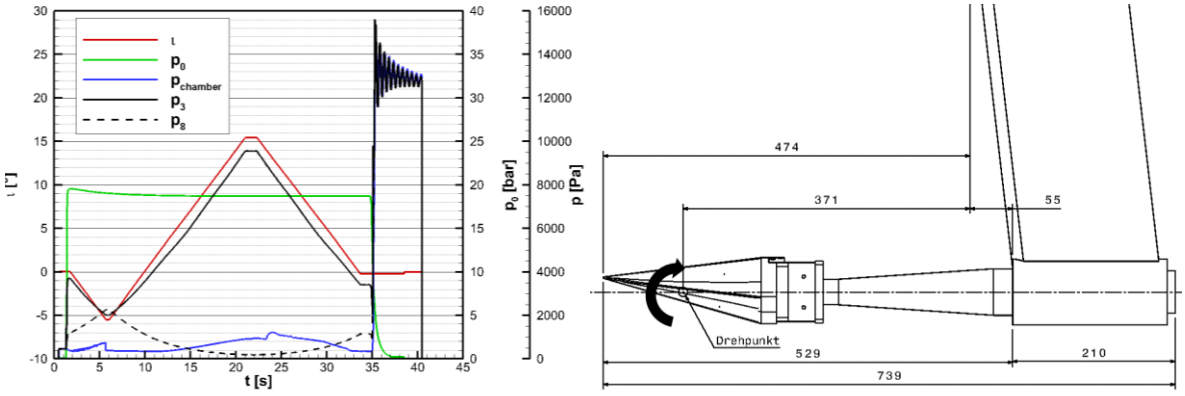

Fig 5: Test procedure and model rotation point in TMK

In the H2K wind tunnel in total 37 runs at Mach numbers 7.0, 6.0 and 5.3 where performed. For the highest Mach number, the Reynolds number was varied between $2 \cdot 10^6$ 1/m to $8 \cdot 10^6$ 1/m. Angle of attack and sideslip were varied as described before.

In the TMK wind tunnel in total 15 runs were performed at Mach numbers of 1.5, 2.0, 3.0 and 4.0. Additional runs were performed for flow visualization using oil film flow technique.

2.5. Numerical simulations

In order to validate the data from the experiments numerical simulations for dedicated points of the wind tunnel runs were performed and are plotted in the following graphs. As solver the DLR Tau code was used with a laminar isothermal wall condition. Since it was not the intention of this study to compare wind tunnel data and numerical simulation the results were used as validity check.

3. Results

3.1. Angle of attack variation and general flow topology

In Fig 6 the typical result of one test is plotted for each sensor data depending on the angle of incident (which is directly correlates with angle of attack). The behavior is basically in accordance with the expected results. The pressure on the bottom (wind side) increases with increasing angle of attack and decreases on the top side (lee side). Each sensor thereby shows a different behavior which allows a determination of the angle of attack from the pressure data. Especially the central most forward sensors 6 and 10 show a very linear behavior for angles up to ±5° which indicates a minor influence of 3-dimensional flow effects around the nose cone and will be therefore important for angle of attack determination. Sensors 3 and 8 further downstream are also linear but slightly less sensitive to angle of attack variations. All other sensors, especially sensor 1 and 5, are more affected by the flow effects around the leading and side edges of the nose and sensitive to sideslip.

The uncertainties are also plotted in this figure and clearly indicate the higher accuracy on the wind side due to the higher local angle of attack, stronger shock and therefore higher pressure.

Some discrepancies to the predictions were found and possible explanations are mentioned directly below:

1) Very small hysteresis effect which is in the uncertainty range of the measurements
   a. Unknown aerodynamic effects
   b. Hysteresis of actuator or angle measurement unit
2) Sensor 1 and 5 should show a similar curve but sensor 5 sees slightly higher pressure
   a. Manufacturing uncertainties

b. Alignment uncertainties

3) Sensor 7 and 9 should show a similar curve but sensor 7 sees slightly lower pressure

a. Same as 2)

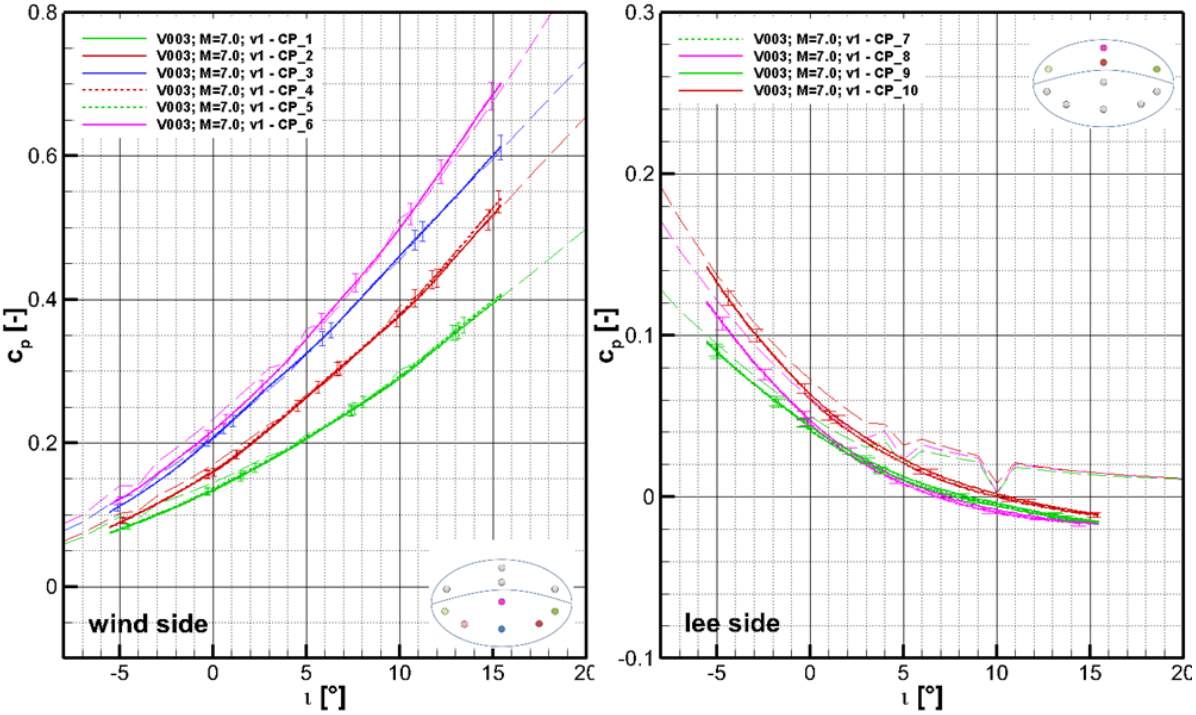

Fig 6: Pressure coefficient for Run 3 in H2K at Mach 7

Fig 7 shows the Schlieren images for ι = 0°, -5° and +5°. In all pictures the bow shock of the horizontal leading edge is visible. Additionally smaller shocks are visible behind the strong bow shock which most likely emerges from the swept leading edges on the side. Generally the flow on the nose cone is quite smooth and no perturbations are visible. After the conical part, the sting mounting of the model generates multiple weak shocks but they do not show an upstream influence.

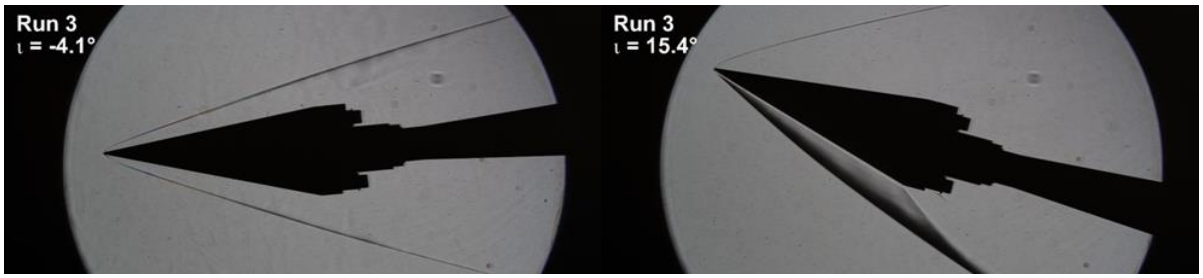

Fig 7: Schlieren images for Run 3 in H2K at Mach 7

For an angle of ι = -5° the local angle of attack on the upside (11°) is nearly the same as on the downside (12°) and the flow looks quite symmetrical. Whereas for ι = +5° the shock on top seems to be separated into two different shocks. This behavior is also visible at ι = 0°.

3.2. Angle of Sideslip Variation

The variation of the sideslip angle shows a very symmetric behavior which indicates a nearly perfect alignment of the model in Figure 34. Some wobbles occur on the measured data on the wind side pressure ports.

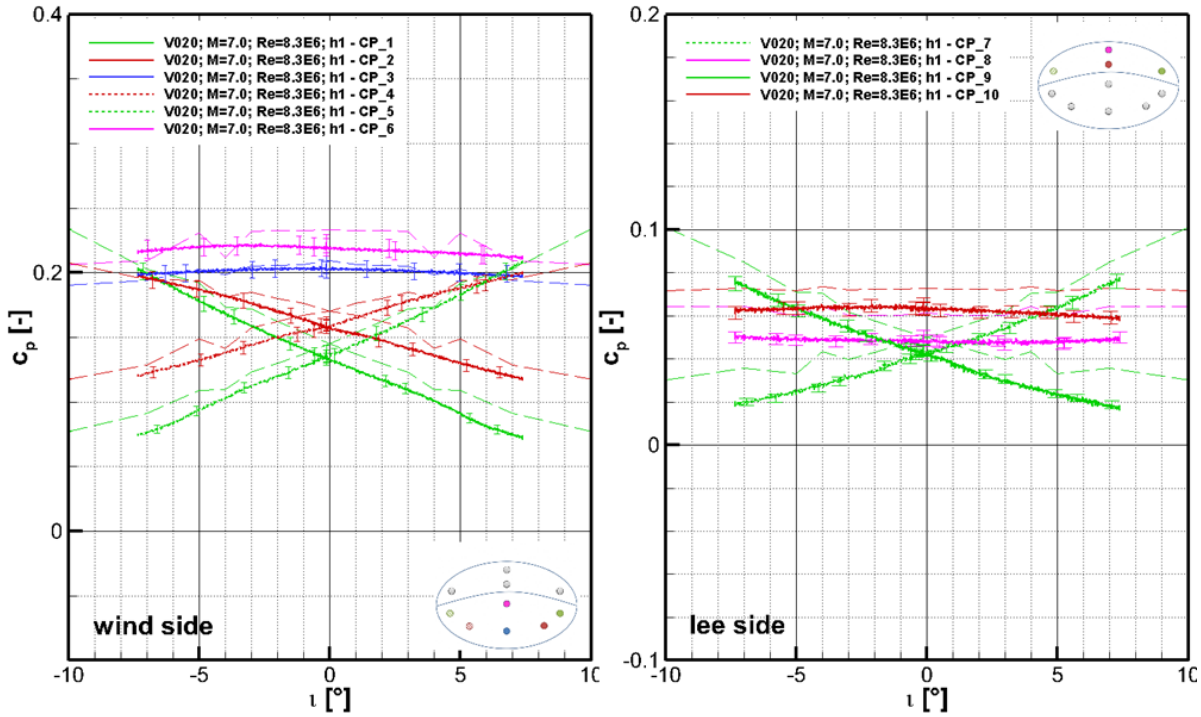

Fig 8: Pressure coefficient for Run 20 at H2K

The difference between CFD data and measured data is quite strong and couldn't be identified within this analysis. It basically shows a similar behavior of the graphs but with a significant offset. Since the measured data on the wind side is higher and too low on the lee side it is possible that the actual angle of attack is slightly higher than 0° as assumed in the CFD. Also it seems that the CFD simulation is not fully converged and "jumps" between different solutions at different angle of sideslips.

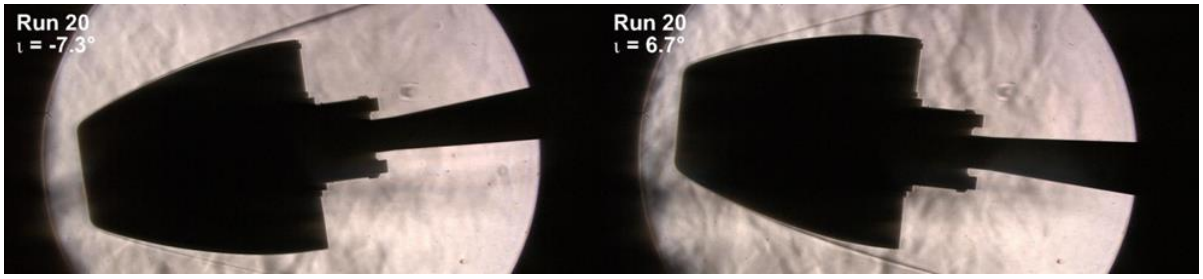

Fig 9: Schlieren images for sideslip variation for Run 20 at H2K

3.3. Mach Number Influence

The influence of Mach number is quite strong on the pressure curve and is plotted for different Mach numbers in Fig 10. Here the pressures on the wind side (left) and lee side (right) is plotted for increasing Mach number from 1.5 to 4.0 whereas lighter lines indicate lower Mach numbers. Interesting to notice is the strong influence of the Mach number on the most upwind sensors P6 and P10 where a significant drop of the pressure coefficient with increasing Mach number is visible. For other sensors this drop is also visible but at a smaller scale. This effect is useful to quantify the Mach number effect on the measurement and helps the FADS to determine the flight velocity.

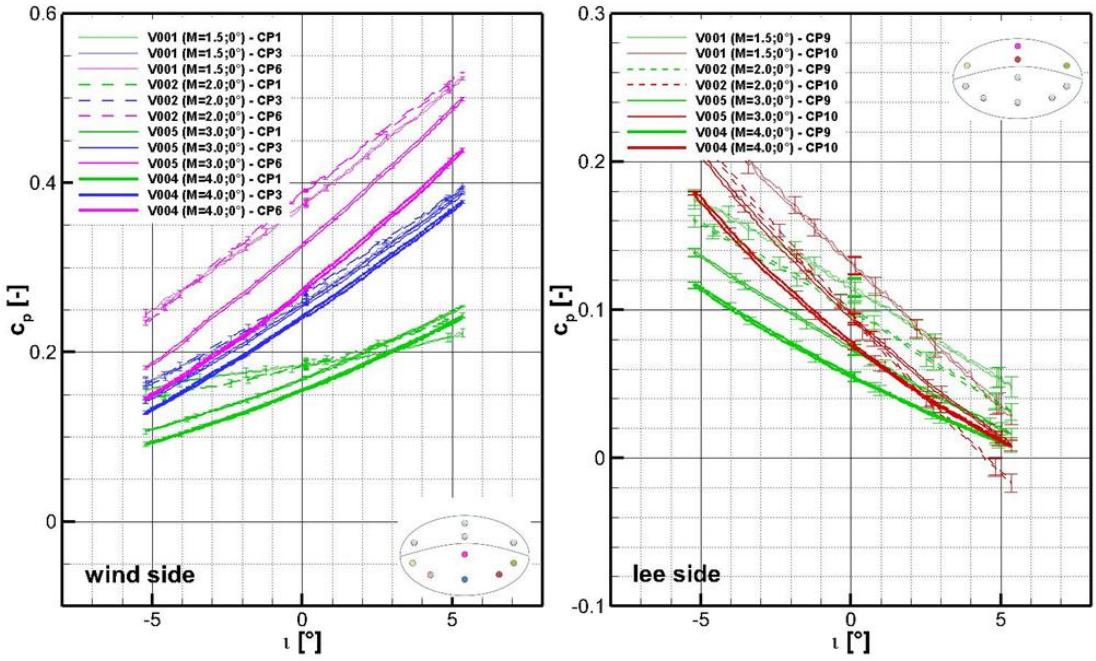

Fig 10: Pressure measurements for different Mach numbers in TMK

A changing Mach number for the runs in the H2K had only minor effects on the behavior of the plots which can be seen exemplary for the angle of attack variation at Fig 11. Remarkable is the difference of the pressure coefficient for high angle of attack at Mach 7 in comparison to other Mach numbers in the CFD data. Some jumps in the data at different angles of attack indicate that there is maybe another possible solution from the CFD for that Mach number. Further CFD needs to be performed to identify this behavior.

In the following Fig 12 the pressure coefficient for 4 sensors on the symmetry plane of the vehicle in each case 2 on the wind and 2 on the lee side are plotted along the Mach number for no angle of attack and sideslip. It shows the consistency of the values for both wind tunnels, whereas the conditions are not directly comparable since the condition in the TMK is operated at a significant higher Reynolds number.

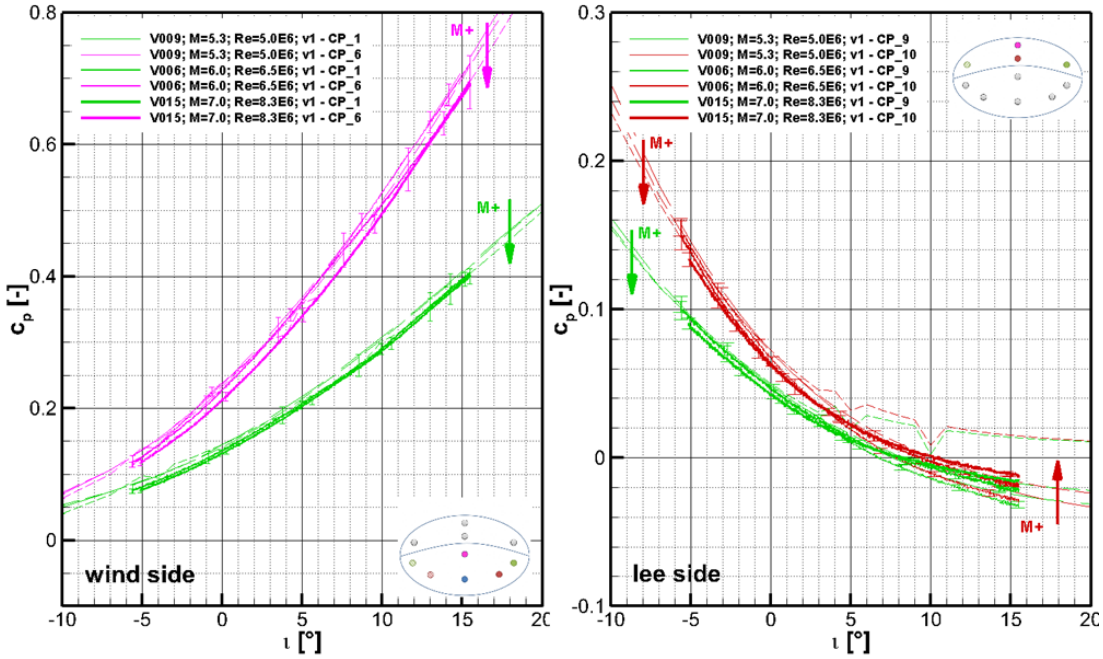

Fig 11: Pressure measurements for different Mach numbers in H2K

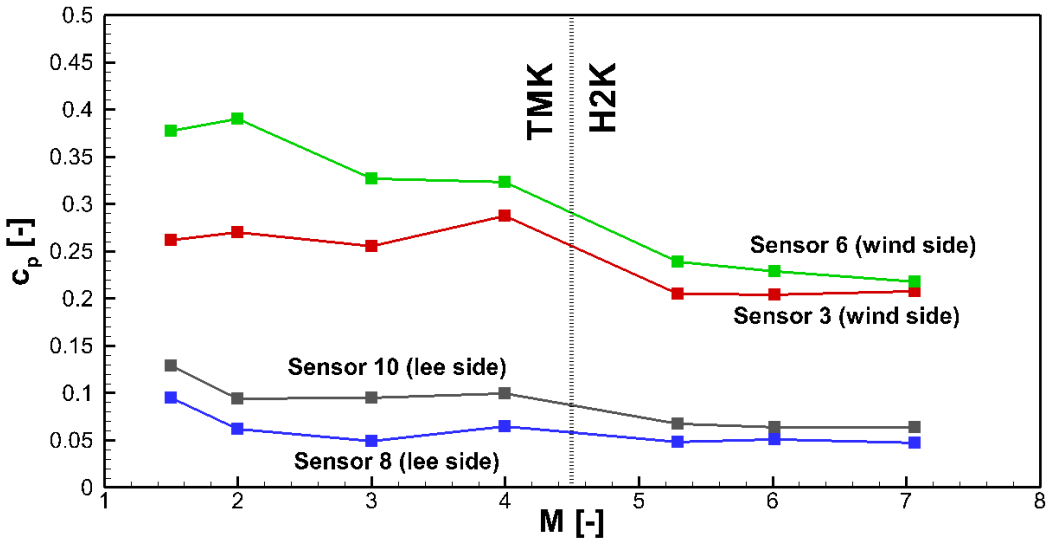

Fig 12: Pressure coefficient for dedicated sensors for different Mach numbers

3.4. Reynolds Number Variation

To evaluate the influence of the Reynolds number in the TMK the ejector system was used which allowed a reduction of back pressure and reducing the allowable static pressure in the test chamber. This way the Reynolds number could be nearly halved but still was higher than for the expected conditions at real flight. Only 2 tests at Mach 2 and Mach 4 with angle of attack variation were performed and are plotted in Fig 13. The shape and behavior do not change with variation of the Reynolds number, only an offset is visible. For the not plotted Mach 4 case the difference between the both Reynolds conditions is hereby slightly higher. The signals of the low Reynolds number conditions are slightly noisier which is caused on one hand by the harsh condition for the wind tunnel and on the other hand by the higher uncertainties due to the lower static pressures on the model.

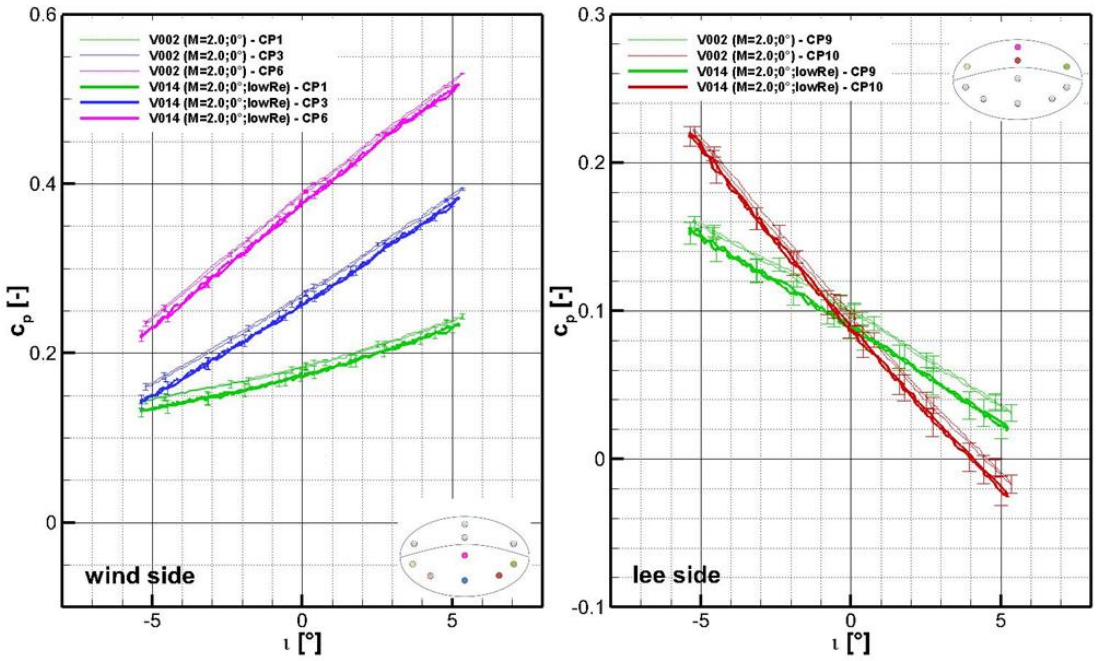

Fig 13: Reynolds number influence at Mach 2

A comparison of the Schlieren images also shows no significant differences in the flow topology. The discrepancies are mainly due to the higher density of the high Reynolds number flow.

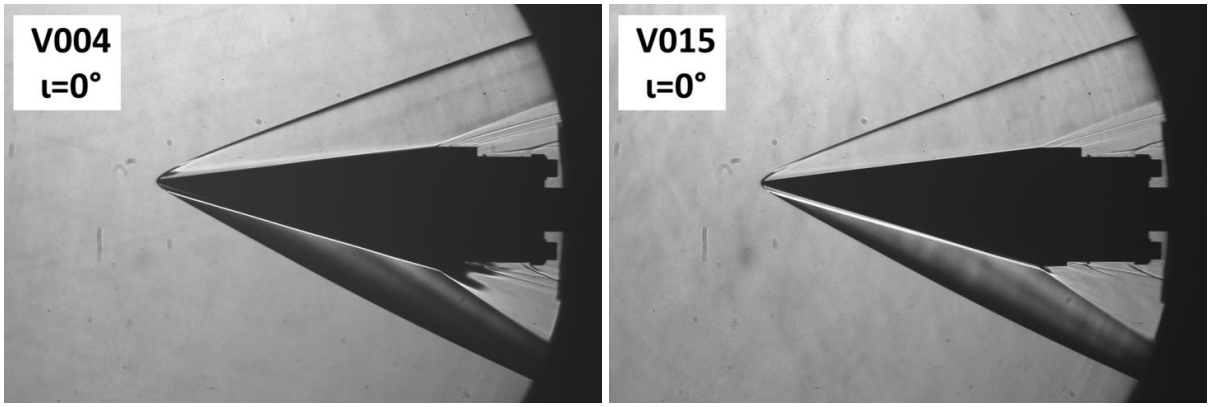

Fig 14: Schlieren images for different Reynolds numbers at Mach 4

At the H2K facility the Reynolds number variation was only performed at Mach 7 for 3 different Reynolds numbers between 2.5mio and 9mio. The results are plotted in Fig 15 and show a significant less important influence on the pressure polar curves.

The Reynolds number observation showed that the influence of the Reynolds number is quite small and can be neglected for coarse determination of the flow angles of the FADS. In contrast and for detailed investigations it is critical to analyze this effect more in detail in order to get fine results. The difficulty is here also that the differences are in the order of the uncertainty of the measurement.

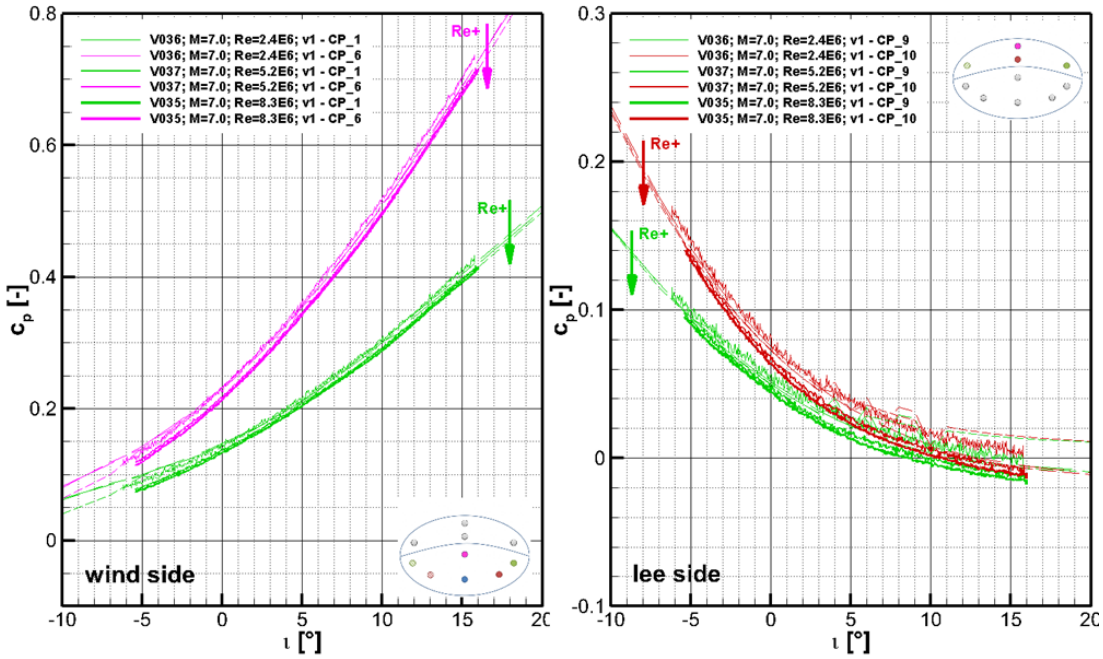

Fig 15: Influence of Reynolds number at Mach 7 in the H2K

3.5. Flow Separation

During the test, the air which hit the model was partially spilled into the test chamber and not sucked by the diffusor. This lead to an increasing pressure in the chamber and hence in an overexpansion of the wind tunnel nozzle. If this effect becomes too strong, it can result in flow separation on the upper side of the model. Since flow separation is very sensitive to a lot of

For the investigated model the effect of overexpansion or even flow separation in the nozzle occur and is clearly visible in the data for a few investigated configuration and has an impact on the validity of the results. Nevertheless the data will be shown and discussed in order to present complete results. But these effects result in further flow field changes which need to be considered when evaluating the data.

Figure 30 shows an example of a run where this effect occurs. The pressure on the top (p8) suddenly increases drastically and proportional to the chamber pressure and shows some hysteresis effect (more likely: memory effect) of the flow. It is assumed that for the high angle of attack the spillage is increased and lead to an increased chamber pressure. As soon as a certain point is exceeded, the flow in the nozzle is significantly overexpanded or even partially separated (this process is still not fully understood and under investigation) and lead to further chamber pressure increase. Since the model is connected with a sting to the chamber it "sees" the higher pressure despite the supersonic flow. On top of the model, the pressure is lower than the chamber pressure and this could trigger boundary layer separation.

Figure 31 shows the schlieren images of the flow shortly before (left) and after (right) the events. The blue arrows mark the shocks coming from the overexpansion or nozzle separation. The red arrow indicates an additional shock which may be caused by a flow separation bubble, which could not directly observed in the schlieren images.

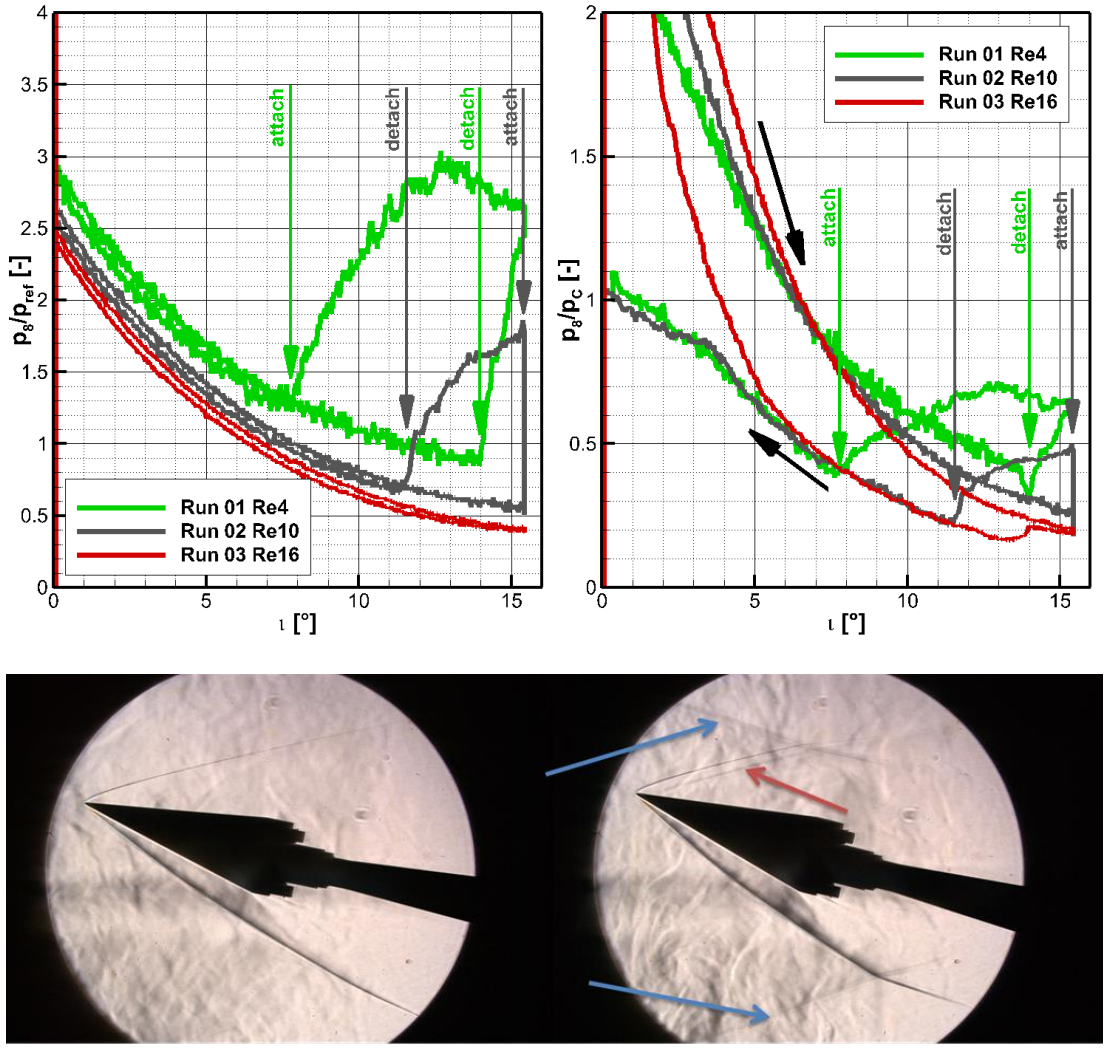

4. Conclusion

A full dataset for the calibration of the FADS for Mach numbers between 1.5 and 7, angle of attack between -5° and +15° and angle of sideslip between -5° and +5° was created. The results show a reasonable good agreement with CFD simulations and the expected trends.

General observations are:

- Pressure is strongly dependent on angle of attack and sideslip for the investigated sensor positions

- Mach number influence is small for hypersonic conditions (Ma>=5.3)
- Reynolds number influence is small
- No hysteresis effects were observed
- Uncertainties are relative small and results show good repeatability

First analysis of the data indicates a good choice for the sensor positions. It also shows that Mach number approximation of the real flight FADS will be connected with higher uncertainties while the pressure coefficients are quite sensitive to angle of attack and sideslip variations.

The results of this study will be used to create a FADS for the flight. The upcoming task (in another work package) will be the comparison of this database with different numerical and analytic tools and creation of correction factors in order to improve the uncertainties and develop an algorithm for fast evaluation of flight speed, ambient pressure, angle of attack and sideslip.

References

1. Baumann, Ethan, et al. "X-43A flush airdata sensing system flight-test results." Journal of Spacecraft and rockets 47.1 (2010): 48-61.
2. Guelhan, Ali. "Main Achievements of the Rocket Technology Flight Experiment ROTEX-T." 21st AIAA International Space Planes and Hypersonics Technologies Conference. 2017.
3. Thiele, Thomas, Dominik Neeb, and Ali Gülhan. "Post-Flight Hypersonic Ground Experiments and FADS Flight Data Evaluation for the SHEFEX-II Configuration." Proceedings of 8th European Symposium on Aerothermodynamics for Space Vehicles. 2015.
4. Schleutker, Thorn, et al. "ExoMars Flush Air Data System: Experimental and Numerical Investigation." *Journal of Spacecraft and Rockets* (2019): 1-12.
5. Steelant, Johan, et al. "Conceptual Design of the High-Speed Propelled Experimental Flight Test Vehicle HEXAFLY." 20th AIAA International Space Planes and Hypersonic Systems and Technologies Conference. 2015.
6. J. Steelant, V. Villace, A. Kallenbach, A. Wagner, J.-Y. Andro, S. di Benedetto, B. Saracoglu, S.L. Chernyshev, A.A. Gubanov, V.A. Talyzin, N.V. Voevodenko, N.V. Kukshinov, A.N. Prokhorov, N. V. Grigoriev, A.J. Neely, D. Verstraete and D. Buttsworth, Flight Testing Designs in HEXAFLY-INT for High-Speed Transportation', 1st International Conference on High-Speed Vehicle Science and Technology (HiSST), 26-29/11/2018, Moscow, Russia.
7. Sitz, Joel R. "The F-18 systems research aircraft facility." (1992).
8. Whitmore, Stephen, Brent Cobleigh, and Edward Haering, Jr. "Design and calibration of the X-33 flush airdata sensing (FADS) system." 36th AIAA aerospace sciences meeting and exhibit. 1998.